PERGAMON

International Journal of Heat and Mass Transfer 43 (2000) 191–201

International Journal of HEAT and MASS TRANSFER

www.elsevier.com/locate/ijhmt

Power extraction from a hot stream in the presence of phase change

J.V.C. Vargas, J.C. Ordóñez, A. Bejan*

Department of Mechanical Engineering and Materials Science, Duke University, Box 90300, Durham, NC 27708-0300, USA

Received 17 September 1998; received in revised form 19 April 1999

Abstract

This paper considers the basic thermodynamic optimization problem of extracting the most power from a stream of hot exhaust when the contact heat transfer area is fixed. It shows that when the receiving (cold) stream boils in the counterflow heat exchanger, the thermodynamic optimization consists of locating the optimal capacity rate of the cold stream. At the optimum, the cold side of the heat transfer surface divides itself into three sections: liquid preheating, boiling and vapor superheating. Numerical results are developed for a range of design parameters of applications with either water or toluene on the cold side. It is shown that the optimal design is robust, because several of the design parameters have only a weak effect on the optimal design.

1. Introduction

In this paper we consider the basic thermodynamics problem of how to extract maximum mechanical power from a stream of hot exhaust. The problem is stated graphically on the left side of Fig. 1. Given is the single-phase stream of hot exhaust, which has the mass flow rate $\dot{m}$ and the initial temperature T_H. This fluid behaves as an ideal gas with nearly constant c_P. The temperature of this stream decreases as it serves as heat input to a power plant. The objective is to maximize the power output $\dot{W}$, or to minimize the total rate of entropy generation of the power plant.

In most power plant designs today, the component that receives the heat input is the duct that carries the working fluid (e.g., water) of the power plant, i.e., the fluid that later completes the power cycle. This component is highlighted on the right side of Fig. 1. The mass flow rate of this second stream, $\dot{m}_w$, is not fixed. The transfer of heat from the hot gas to the water stream occurs across a heat transfer surface of area A, which is fixed. The temperature difference across this surface is responsible for the irreversibility of the $\dot{m}/\dot{m}_w$ heat exchanger: this irreversibility leads to a decrease in the power output of the plant. In order to isolate and minimize the stream-to-stream heat transfer irreversibility, we model the rest of the power plant as a reversible compartment. The pressure drops experienced by $\dot{m}$ and $\dot{m}_w$ are assumed negligible.

The thermodynamic optimization problem amounts to finding the best 'match' between $\dot{m}$ and $\dot{m}_w$, across A. This problem is challenging for several reasons. First, the water stream may experience a change of phase (vaporization) over an intermediate section of the heat exchanger, where the water temperature remains constant. In this case the spatial distribution of the $\dot{m}_w$ stream temperature exhibits sharp changes in slope (e.g., Fig. 2 later in this paper), and cannot be

* Corresponding author. Tel.: +1-919-660-5310; fax: +1-919-660-8963.

E-mail address: abejan@duke.edu (A. Bejan)

0017-9310/00/$ - see front matter
PII: S0017-9310(99)00146-5

Nomenclature

a, b	dimensionless groups of thermophysical properties, Eqs. (35) and (36)
A	area, m^2
c_s	specific heat of steam at constant pressure, J/kg K
$\bar{c}_s$	average specific heat of steam at constant pressure, J/kg K
c_P	specific heat of hot gas at constant pressure, J/kg K
c_w	specific heat of liquid water, J/kg K
e_x	specific flow exergy, J.kg
h_{fg}	specific latent heat, J/kg
$\dot{m}$	mass flow rate of hot gas, kg/s
$\dot{m}_w$	mass flow rate of cold stream, kg/s
M	ratio of mass flow rates, Eq. (38)
N	number of heat transfer units
P	pressure, Pa
$\dot{Q}_0$	rate of heat rejection to the ambient, W
$\dot{Q}_e$	heat transfer rate during thermal mixing with the ambient, W
s	specific entropy, J/kg K
$\dot{S}_{gen}$	entropy generation rate, W/K
T	temperature, K
T_0	ambient temperature, K
U	overall heat transfer coefficient, W/m^2 K
$\dot{W}$	power, W
x, y	area fractions, Eq. (25)

Greek symbols

ϵ	heat exchanger effectiveness
η_{II}	second law efficiency
μ, μ'	ratios of capacity rates, Eqs. (5) and (12)
τ	dimensionless temperature, T/T_0

Subscripts

b	boiling section
f	saturated liquid
g	saturated vapor
H	hot stream inlet
out	hot stream outlet
s	superheated steam
w	liquid stream
1, 2, 3, 4	states defined on Fig. 2

forced to match the smooth distribution of the hot-gas temperature.

The second complication is introduced by the heat transfer surface A. The heat transfer coefficient is fairly easy to predict for the hot side of A, because the $\dot{m}$ stream is single-phase, and the heat transfer characteristics of ideal gases are well known. On the cold side, the heat transfer surface is actually a succession of three sections, the surface A_w over which the liquid water is heated to the boiling point, the surface A_b over which the $\dot{m}_w$ stream boils, and finally, the surface A_s that superheats the steam. The simplicity of the total heat transfer surface constraint

$$A = A_w + A_b + A_s \tag{1}$$

is deceiving, because the cold side of each section has its own heat transfer coefficient. This means that each section is also characterized by distinct overall (stream-to-stream) heat transfer coefficient, namely U_w over the A_w section, U_b over the boiling section A_b, and U_s over the superheating section A_s.

The third complication is the heart of the thermodynamic optimization problem: the flow rate $\dot{m}_w$ is not specified. How fast should the power-plant working fluid be circulated through the heat exchanger? To see the importance of this question, consider the two extremes. In the limit $\dot{m}_w \to 0$, the final temperature reached by the water steam is maximum (T_H), but the exergy flow rate carried by this stream vanishes because $\dot{m}_w$ vanishes. Consequently, $\dot{W}$ approaches zero because its only exergy source is the exergy brought by the $\dot{m}_w$ stream into the reversible compartment. In the opposite limit, $\dot{m}_w \to \infty$, the final temperature of the water stream is nearly equal to its initial temperature. Consequently, the flow exergy acquired by the $\dot{m}_w$ stream approaches zero, and so does the power output $\dot{W}$. These asymptotes suggests that there might exist an intermediate flow rate $\dot{m}_w$ that optimizes the match between the hot exhaust and the power plant.

The following analysis describes our search for this optimal match. We seek more than the optimal ratio $\dot{m}_w/\dot{m}$ for a given set of constraints (A, U_w, U_b, U_s, T_H, T_0). More important is the strategy that we must follow in order to minimize the entropy generated during the stream-to-stream interaction. Strategy means how to distribute the stream-to-stream irreversibility (e.g., temperature gaps) in space, and how to allocate A among the three sections (A_w, A_b, A_s). Strategy also requires an understanding of the 'robustness' of the optimization results that will be determined. Are these results sensitive to changes in every single constraint and parameter? For example, one parameter is the type of working fluid (Section 6). The constrained parameters that have the greatest impact on the thermodynamic optimum are the most import-

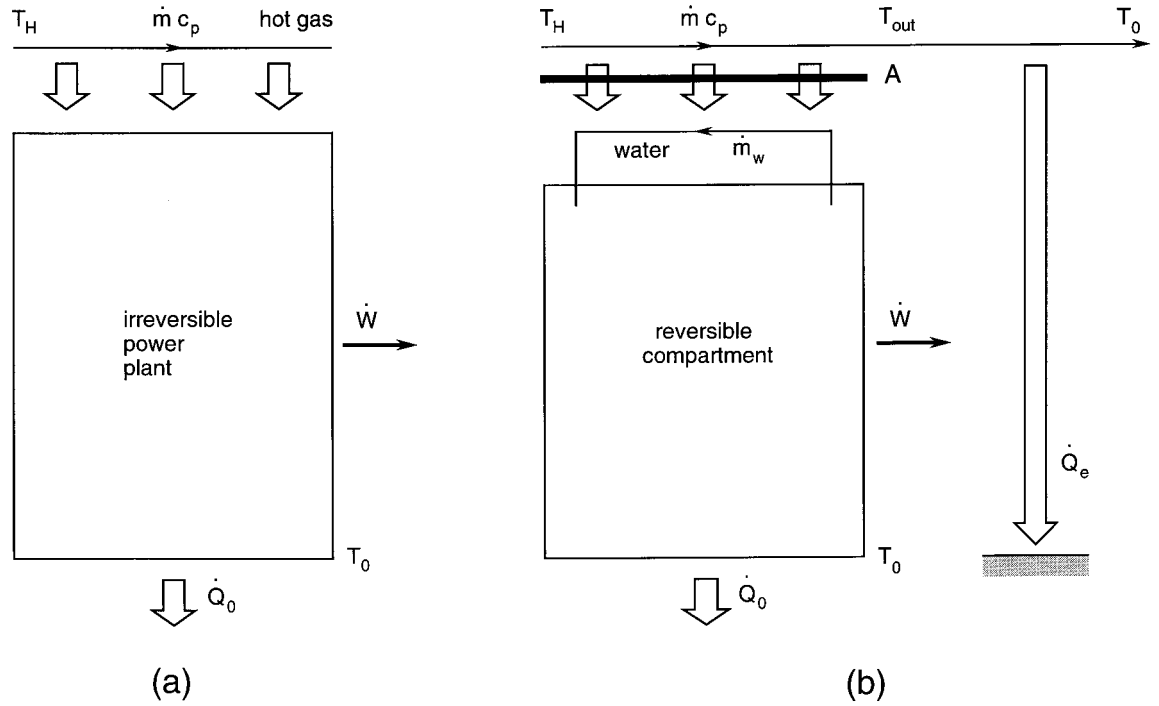

Fig. 1. The extraction of power from a stream of hot exhaust.

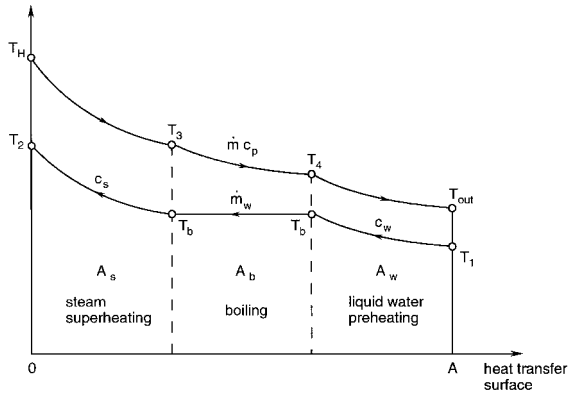

Fig. 2. The two temperature distributions along the three sections of the counterflow heat exchanger of Fig. 1(b).

ant, and to identify them and their impact early is the best strategy.

2. Heat transfer analysis

The method of entropy generation minimization (EGM) combines thermodynamics with the transport (heat transfer) characteristics of the irreversible system. The objective of the heat transfer analysis is to determine a meaningful relation—a function—between the entropy generation rate and the physical parameters and constraints of the modeled system (e.g., finite sizes, materials). In the end, this function is used in order to determine the optimal physical characteristics that lead to minimum entropy generation at the system level.

The heat transfer analysis of the heat exchanger formed by $\dot{m}$ and $\dot{m}_w$ can be outlined with reference to Fig. 2. The hot gas stream and the water stream run in counterflow. We assume that the water enters as a subcooled liquid (T_1, P_1). When the water flow rate is sufficiently small, the water stream boils completely and is superheated before leaving the heat exchanger (T_2, P_2). In this case the three sections of the water side of the heat transfer surface divide the system into three sequential counterflow heat exchangers. These are indicated by A_w, A_b and A_s in Fig. 2.

The heat transfer functioning of each heat exchanger is described by the classical effectiveness—NTU relations [1]. Proceeding from left to right in Fig. 2, we start with the superheater (T_h, T_3, T_b, T_2) for which the effectiveness relations are

$$\epsilon_s = \frac{1-\exp[-N_s(1-\mu)]}{1-\mu\,\exp[-N_s(1-\mu)]} \tag{2}$$

$$\epsilon_s = \frac{T_H - T_3}{\mu(T_H - T_b)} \tag{3}$$

$$\epsilon_s = \frac{T_2 - T_b}{T_H - T_b} \tag{4}$$

where

$$\mu = \frac{\dot{m}_w c_s}{\dot{m} c_P} \quad N_s = \frac{U_s A_s}{\dot{m}_w c_s} \tag{5}$$

and c_s is the specific heat at constant pressure for steam. According to heat exchanger theory, Eqs. (2)–(5) are valid when the hot gas has the larger capacity rate, i.e., when $\mu < 1$. The opposite case ($\mu > 1$) is described by a similar set of equations, which are omitted here for the sake of conciseness. Continuing with Eqs. (3) and (4), we can express T_3 and T_2 as functions of the extreme end temperatures:

$$T_3 = T_H - \mu\epsilon_s(T_H - T_b) \tag{6}$$

$$T_2 = T_b + \epsilon_s(T_H - T_b) \tag{7}$$

In the boiling section the temperature on the cold side is uniform, T_b. The effectiveness–NTU formulation for this section is represented by [1]

$$\epsilon_b = 1 - \exp(-N_b) \tag{8}$$

$$T_4 = T_3 - \epsilon_b(T_3 - T_b) \tag{9}$$

where

$$N_b = \frac{U_b A_b}{\dot{m} c_P} \tag{10}$$

The first law of thermodynamics for the boiling section, $\dot{m}_w h_{fg} = \dot{m} c_P (T_3 - T_4)$, yields a second relation between T_3 and T_4:

$$T_3 - T_4 = \mu \frac{h_{fg}}{c_s} \tag{11}$$

Finally, in the water preheating section the capacity rates are $\dot{m} c_P$ and $\dot{m}_w c_w$, where c_w is the specific heat of liquid water. We define the capacity rate ratio

$$\mu' = \frac{\dot{m}_w c_w}{\dot{m} c_P} = \mu \frac{c_w}{c_s} \tag{12}$$

and assume that $\mu' < 1$. The effectiveness–NTU formalism reduces to

$$\epsilon_w = \frac{1 - \exp[-N_w(1 - \mu')]}{1 - \mu' \exp[-N_w(1 - \mu')]} \tag{13}$$

$$T_{out} = (1 - \mu'\epsilon_w)T_4 + \mu'\epsilon_w T_1 \tag{14}$$

$$T_4 = T_1 + \frac{1}{\epsilon_w}(T_b - T_1) \tag{15}$$

where

$$N_w = U_w A_w / (\dot{m}_w c_w) \quad (\mu' < 1) \tag{16a}$$

$$N_w = U_w A_w / (\dot{m} c_P) \quad (\mu' > 1) \tag{16b}$$

In summary, the complete heat exchanger is described by a total of nine equations: three effectiveness–NTU equations [namely, Eqs. (2), (8) and (13)] plus six equations containing the end temperatures of the three sections [namely, Eqs. (6), (7), (9), (11), (14), and (15)]. The latter can be made dimensionless by referencing all the temperatures to the ambient temperature ($\tau_i = T_i/T_0$):

$$\tau_3 = \tau_H - \mu\epsilon_s(\tau_H - \tau_b) \tag{17}$$

$$\tau_2 = \tau_b + \epsilon_s(\tau_H - \tau_b) \tag{18}$$

$$\tau_4 = \tau_3 - \epsilon_b(\tau_3 - \tau_b) \tag{19}$$

$$\tau_3 = \tau_4 + \mu \frac{h_{fg}}{c_s T_0} \tag{20}$$

$$\tau_{out} = (1 - \mu'\epsilon_w)\tau_4 + \mu'\epsilon_w\tau_1 \tag{21}$$

$$\tau_4 = \tau_1 + (\tau_b - \tau_1)/\epsilon_w \tag{22}$$

To this system of nine equations we add the total surface constraint (1), which now reads

$$N = \mu N_s + \frac{U_s}{U_b} N_b + \mu' \frac{U_s}{U_w} N_w \quad (\mu < 1, \mu' < 1) \tag{23a}$$

$$N = \mu N_s + \frac{U_s}{U_b} N_b + \frac{U_s}{U_w} N_w \quad (\mu < 1, \mu' > 1) \tag{23b}$$

where

$$N = \frac{U_s A}{\dot{m} c_P}, \quad \text{constant} \tag{24}$$

In the numerical implementation of this analysis, it is convenient to account for the constraint (23) by introducing the area fractions

$$x = \frac{A_s}{A} \quad y = \frac{A_b}{A} \quad 1 - x - y = \frac{A_w}{A} \tag{25}$$

such that $x = \mu N_s/N$, $y = (U_s/U_b)N_b/N$ and $1 - x - y = \mu'(U_s/U_w)N_w/N$, when both μ and μ' are less than 1.

3. Entropy generation analysis

There is more than one way in which thermodynamic optimization can be performed. Consider the 'aggregate' system that contains absolutely all the components that are situated at temperatures above T_0. This system includes what is shown in Fig. 1(a) plus the external course followed by $\dot{m}$ as it is dumped into the ambient. During this external thermal mixing, the hot gas transfers $\dot{Q}_e = \dot{m}(h_{out} - h_0)$ into the atmosphere, where the subscript $(\,)_0$ indicates thermomechanical equilibrium with the environment (the restricted dead state [2]). The first law and the second law for the steady-state operation of the aggregate system are

$$\dot{W} = \dot{m}(h_H - h_0) - \dot{Q}_0 - \dot{Q}_e \tag{26}$$

$$\dot{S}_{gen} = \frac{\dot{Q}_0 + \dot{Q}_e}{T_0} + \dot{m}(s_0 - s_H) \geq 0 \tag{27}$$

By eliminating $(\dot{Q}_0 + \dot{Q}_e)$ between these two statements we obtain

$$\dot{W} = \dot{m} e_{x,H} - T_0 \dot{S}_{gen} \tag{28}$$

where $e_{x,H}$ is the initial specific flow exergy of the hot gas, $e_{x,H} = (h_H - T_0 s_H) - (h_0 - T_0 s_0)$. The final flow exergy of the $\dot{m}$ stream is zero, by definition, because at that state $\dot{m}$ reaches thermomechanical equilibrium with the ambient.

Eq. (28) shows that the power output is equal to the flow exergy decrease experienced by the hot stream, minus the product $T_0 \dot{S}_{gen}$ which represents the destroyed exergy. The latter is located in a region containing the $\dot{m}/\dot{m}_w$ heat exchanger and the external portion where $\dot{m}$ is cooled down to T_0. To calculate $T_0 \dot{S}_{gen}$, we write the first law and the second law for this region

$$\dot{m}(h_H - h_0) - \dot{m}_w(h_2 - h_1) - \dot{Q}_e = 0 \tag{29}$$

$$\dot{S}_{gen} = \dot{m}(s_0 - s_H) + \dot{m}_w(s_2 - s_1) + \frac{\dot{Q}_e}{T_0} \geq 0 \tag{30}$$

and eliminate $\dot{Q}_e$ between Eqs. (29) and (30),

$$T_0 \dot{S}_{gen} = \dot{m} e_{x,H} - \dot{m}_w(e_{x,2} - e_{x,1}) \tag{31}$$

Eq. (31) shows that the destroyed exergy is the difference between the exergy brought in by the hot gas and the exergy picked up by the water stream. If we eliminate $T_0 \dot{S}_{gen}$ between Eqs. (28) and (31) we obtain

$$\dot{W} = \dot{m}_w(e_{x,2} - e_{x,1}) \tag{32}$$

which states that the power output is equal to the net flow of exergy into the reversible compartment shown in Fig. 1(b). Eq. (32) could have been obtained directly by writing the first law and the second law for that compartment alone.

The maximization of $\dot{W}$ can be pursued by using either Eq. (28) or Eq. (32). In the former, $\dot{W}$ maximization is achieved through the minimization of the total entropy generation rate, where $\dot{S}_{gen}$ is calculated based on Eq. (30). The second alternative, Eq. (32), is considerably more direct: $\dot{W}$ can be maximized by simply maximizing the flow exergy picked up by the second stream. Since the properties at State 1 are usually fixed by the ambient, or by the design of the power cycle (for example, T_1 is the condensation temperature), the maximization of $\dot{W}$ requires the maximization of the exergy flow rate registered at State 2. This alternative was selected in our numerical work, because it is the simplest.

The proper dimensionless measure of the thermodynamic optimum is the maximum reached by the second law efficiency

$$\eta_{II} = \frac{\dot{W}}{\dot{m} e_{x,H}} = \frac{\dot{m}_w(e_{x,2} - e_{x,1})}{\dot{m} e_{x,H}} \tag{33}$$

The flow exergy change experienced by the water stream is evaluated by considering the three parts of the heat exchanger, $e_{x,2} - e_{x,1} = (e_{x,2} - e_{x,g}) + (e_{x,g} - e_{x,f}) + (e_{x,f} - e_{x,1})$, where $e_x = h - T_0 s$. Eq. (33) can be developed into

$$\eta_{II} = \frac{\mu(a+b)}{\tau_H - 1 - \ln\ \tau_H} \tag{34}$$

where a and b are functions that depend on the model adopted for the properties of steam:

$$a = \tau_2 - \tau_b - \ln\ \frac{\tau_2}{\tau_b} \quad \text{(steam as an ideal gas)} \tag{35a}$$

$$a = \frac{h_2 - h_g}{\bar{c}_s T_0} - \frac{s_2 - s_g}{\bar{c}_s} \quad \text{(tabulated steam properties)} \tag{35b}$$

$$b = \frac{h_{fg}}{\bar{c}_s T_0}\left(1 - \frac{1}{\tau_b}\right) + \frac{c_w}{\bar{c}_s}\left(\tau_b - \tau_1 - \ln\ \frac{\tau_b}{\tau_1}\right) \tag{36}$$

The specific heat of liquid water was based on tabulated data [3] and evaluated at the boiling point, $c_w = c_w(T_b)$. The specific heat at constant pressure of steam was taken as the average of the tabulated values corresponding to the inlet and outlet of the steam section of the heat exchanger, $\bar{c}_s = (1/2)[c_s(T_2) + c_s(T_b)]$.

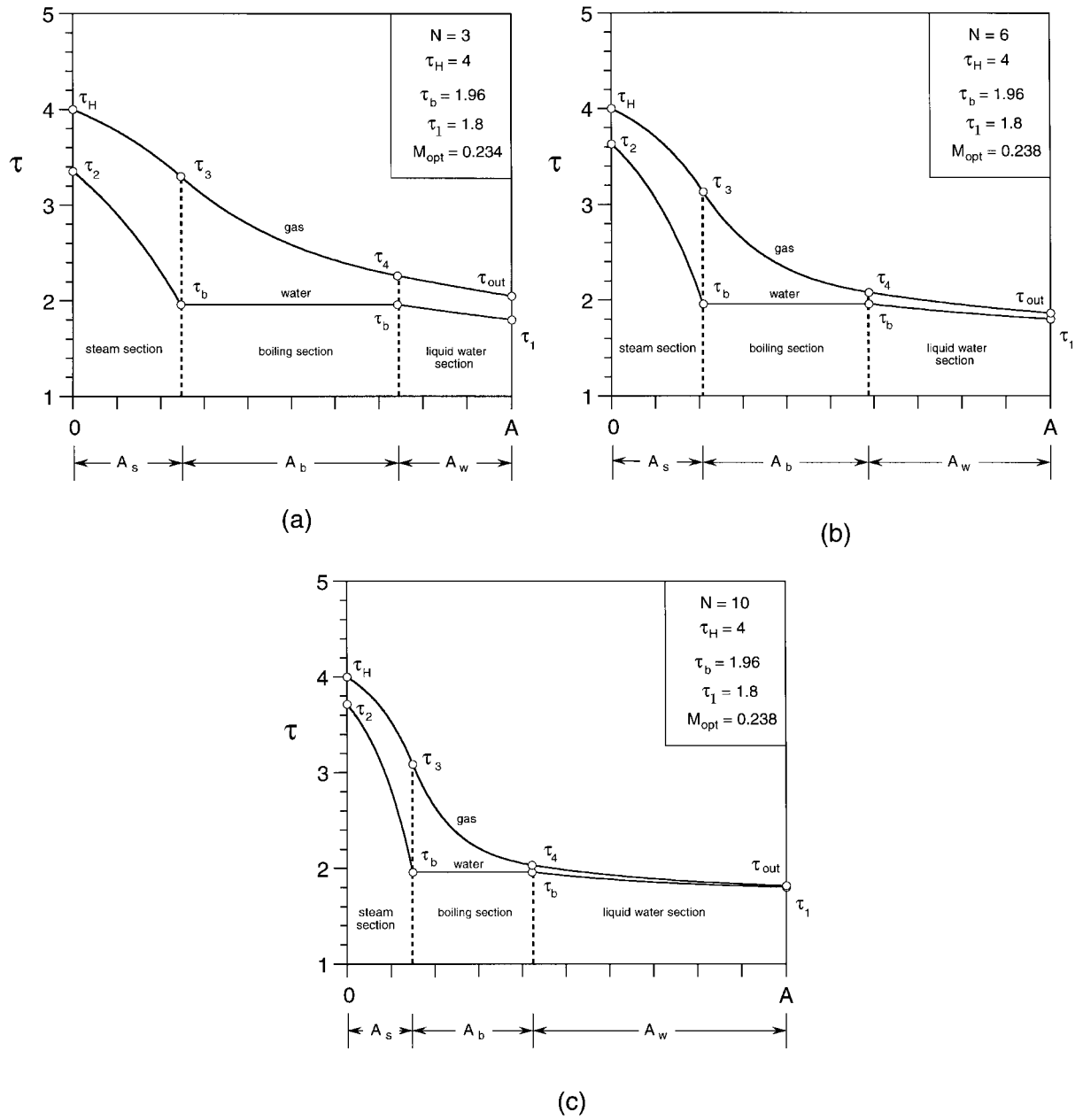

Fig. 3. The effect of the heat transfer area size on the match between the temperature distributions of the two streams.

4. Results for water as the cold stream

Fig. 3a–c shows the actual temperature distribution along the heat exchanger, as the two streams sweep the total area A. This first set of results is for orientation, and is based on the simplifying assumption that the overall heat transfer coefficient has the same value in each of the three sections of the heat exchanger,

$$U_s = U_b = U_w \tag{37}$$

The dimensional end-temperatures for which this figure was constructed correspond to a water stream at 100 bar, which enters as condensate at $T_1 = 537$ K and boils at $T_b = 584$ K. The inlet temperature of the hot gas is $T_H = 1193$ K, and the ambient temperature is $T_0 = 298$ K. The exponential shapes of the segments of

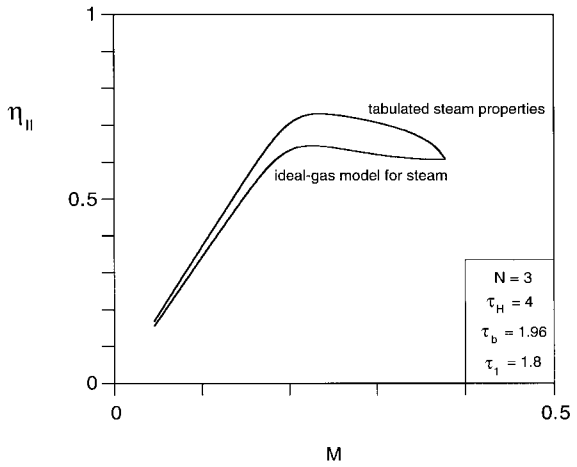

Fig. 4. The maximization of thermodynamic performance by selecting the mass flow rate of the water stream, or the ratio $M = \dot{m}_w/\dot{m}$.

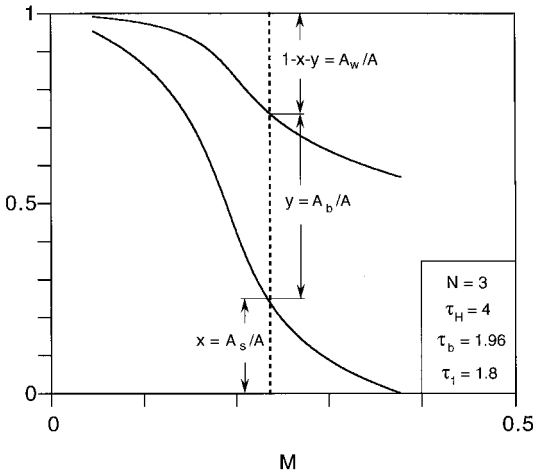

Fig. 5. The effect of the water mass flow rate on the allocation of area among the three sections of the heat exchanger.

the temperature curves follow from the classical solution for counterflow heat exchangers in the effectiveness–NTU formulation. The three graphs of Fig. 3 show that the temperature gap becomes narrower when the overall size of the heat exchanger (N) increases. This effect is analyzed further in Fig. 6.

Each of the frames of Fig. 3 was drawn for a fixed mass flow rate ratio,

$$M = \frac{\dot{m}_w}{\dot{m}} = \mu\frac{c_P}{\bar{c}_s} \tag{38}$$

We found that if we vary M the temperature distributions shift, and the second law efficiency exhibits a maximum at a certain value, M_{opt}. This effect is illustrated in Fig. 4, which also shows that the model adopted for steam properties has a noticeable effect on the optimum ($\eta_{II,max}$, M_{opt}). The numerical results discussed next are based on the tabulated properties of steam. Note that each frame of Fig. 3 was drawn for the M value that maximizes the second law efficiency when N, τ_H, τ_b and τ_l are fixed.

The same effect is pursued further in Fig. 5, where the ordinate shows how the total contact area A is divided between the three sections of the heat exchanger. The sections occupied by liquid water and two-phase flow increase as M increases, and when M exceeds 0.378 the steam section disappears completely. In the case documented in Figs. 3–5 the thermodynamic optimum occurs when all three sections are present, as shown in Fig. 3. The optimum is indicated by the dashed line drawn at $M_{opt} = 0.234$ in Fig. 5.

The existence of the thermodynamic optimum—the optimal ratio M—is fundamental. It means that any stream can be matched optimally to another stream, such that most of the exergy carried originally by the hot stream is captured by the cold stream. In the next phase of this study we examined systematically the effect of the boundary parameters of the arrangement. The purpose of this sensitivity study was to identify the parameters that do not influence the thermodynamic optimum significantly. In other words, we wanted to document the robustness of the results that are based on the optimization of a single case.

This work begins with Fig. 6, which shows how the optimum responds to changes in the overall size of the heat transfer area (N). The key observation concerns $\eta_{II,max}$ and M_{opt}: the optimal thermodynamic performance is practically insensitive to changes in N when N is sensibly greater than five. The relative allocation of

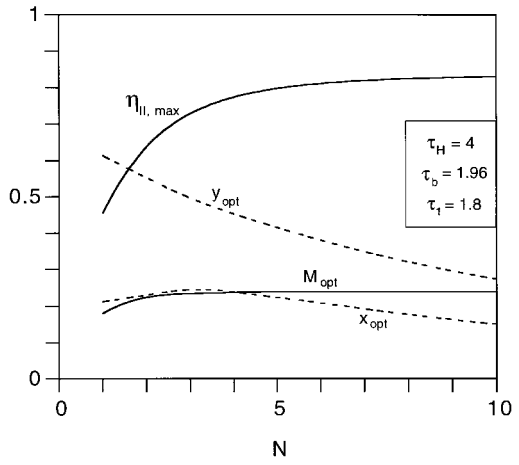

Fig. 6. The effect of the total heat exchanger size (N) on the thermodynamic optimum, and on the allocation of heat transfer area.

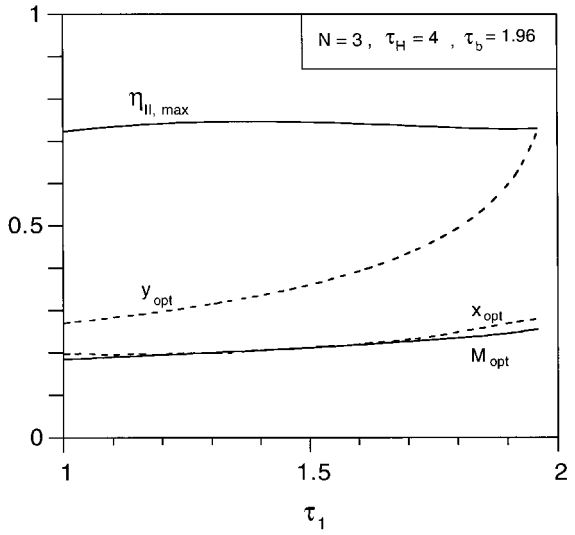

Fig. 7. The effect of the water inlet temperature on the thermodynamic optimum, and on the allocation of heat transfer area.

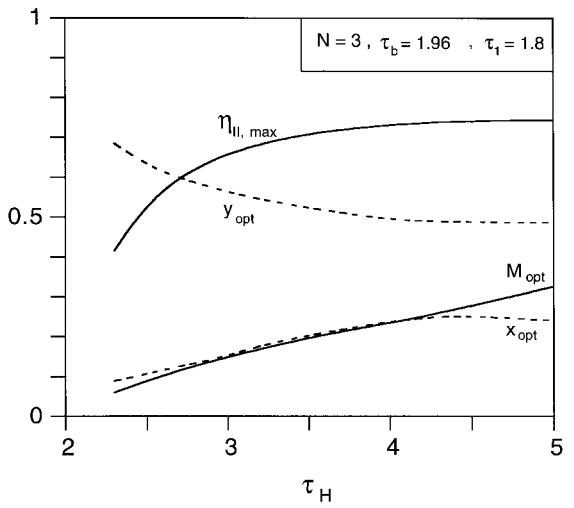

Fig. 8. The effect of the hot-gas inlet temperature on the thermodynamic optimum, and on the allocation of heat transfer area.

heat transfer area continues to respond to increases in N: the area fraction swept by liquid water, A_w (or $1-x-y$), increases monotonically at the expense of both A_b and A_s. The area fraction allocated to the steam section exhibits a maximum at $N\cong 3.18$.

The effect of varying the inlet temperature of the water stream is reported in Fig. 7. The effect of τ_1 on both $\eta_{II,max}$ and M_{opt} is very weak. We conclude that the thermodynamic optimum is robust relative to changes in τ_1. On the other hand, the relative allocation of contact surface is sensitive to τ_1: the liquid–water area decreases monotonically as τ_1 increases, while A_b and A_s increase monotonically.

Fig. 8 shows the effect of the high temperature τ_H on the thermodynamic optimum. All the optimized parameters respond to changes in τ_H. Most significant is the optimal mass flow rate ratio M_{opt}, which increases almost linearly as τ_H increases.

The boiling temperature τ_b has only a weak effect on the optimal mass flow rate ratio, as shown in Fig. 9. The contact area allocated to the boiling section decreases gradually as τ_b increases, and vanishes when τ_b reaches the critical temperature. At this point, more than 80% of the heat transfer area is devoted to superheating the water stream. The maximum second law efficiency increases monotonically as τ_b increases.

We continued the work with water by relaxing the assumption that the overall heat transfer coefficient has the same value in all three sections of the heat exchanger, Eq. (37). Guided by the well-known orders of magnitude of the heat transfer coefficient in various heat transfer regimes [4], we expected $U_b > U_s$ and

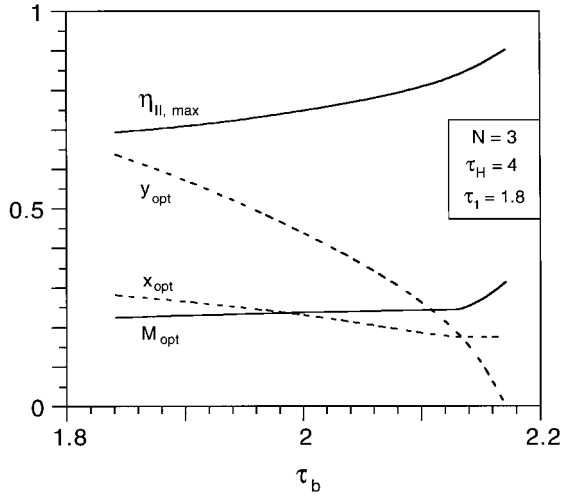

Fig. 9. The effect of the boiling temperature on the thermodynamic optimum, and on the allocation of heat transfer area.

$U_w > U_s$, and considered several cases in the range $1 \le U_b/U_s \le 100$ and $1 \le U_w/U_s \le 10$. The results shown in Fig. 10 indicate that the optimal flow rate ratio and the maximum second law efficiency are relatively insensitive to how the overall heat transfer coefficient varies along the heat exchanger. Changes are felt in the relative lengths of the three sections, as shown in Fig. 11. As expected, the boiling section (y_{opt}) becomes shorter as U_b increases. The superheating and boiling sections (x_{opt}, y_{opt}) increase, and the water preheating section decreases in size, as U_w increases rela-

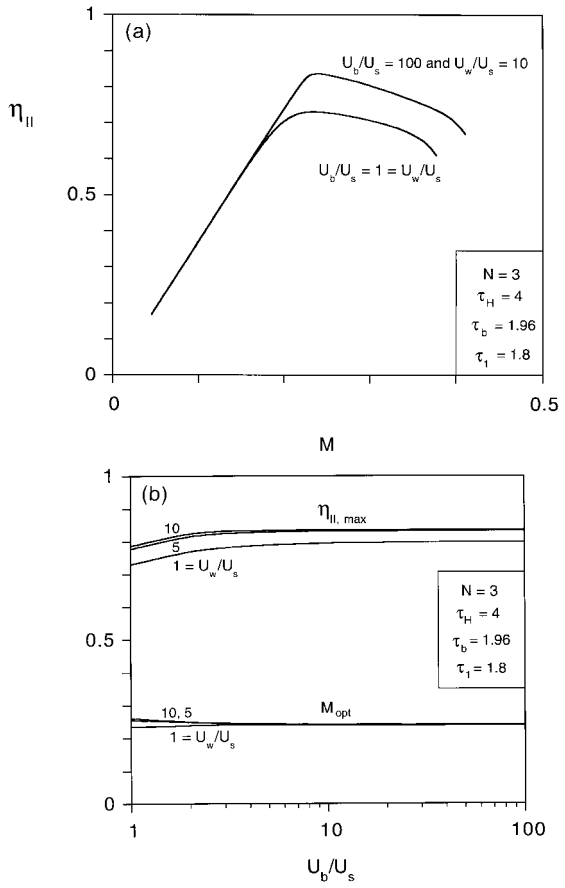

Fig. 10. Different overall heat transfer coefficients for the three sections of the heat exchanger, and their effect on the thermodynamic optimum.

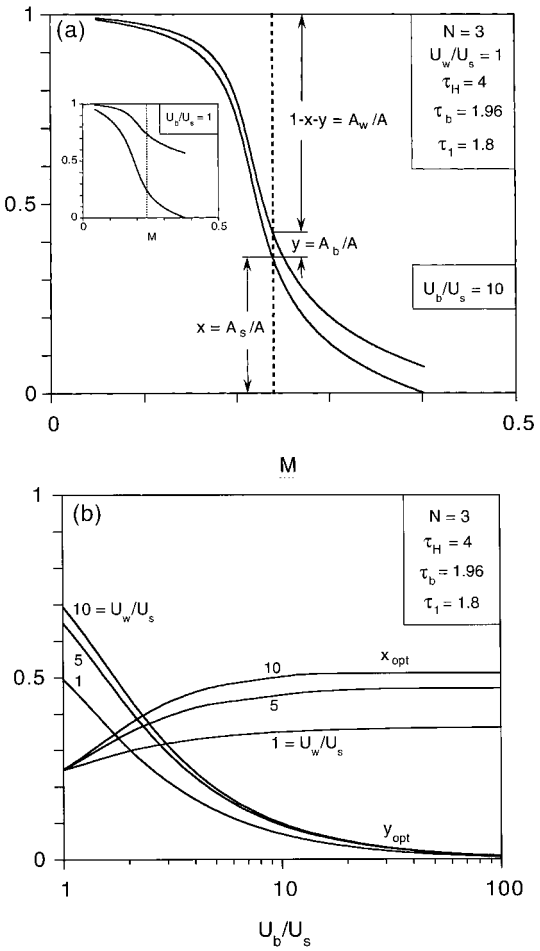

Fig. 11. The effect of the overall heat transfer coefficients on the relative allocation of contact area.

tive to U_s. Taken together, these results show that the thermodynamic optimum (M_{opt}, $\eta_{II,max}$) is robust relative to spatial variations in the overall heat transfer coefficient.

5. Numerical method

The numerical work consisted of solving the nonlinear system of Eqs. (2), (8), (13), (17)–(22) with the objective of maximizing η_{II}. The second law efficiency was determined for a set of fixed parameters: N, τ_H, τ_b, τ_1, M, U_b/U_s and U_w/U_s. The system was solved in two steps: (i) by analytical substitution, after which Eqs. (2), (8) and (13) delivered $x=f_1(\tau_2)$, $y=f_2(\tau_2)$ and $(1-x-y)=f_3(\tau_2)$, respectively, and (ii) by invoking the total surface constraint (1),

$$F(\tau_2) = f_3(\tau_2) - [1 - f_1(\tau_2) - f_2(\tau_2)] \quad (39)$$

and seeking $F(\tau_2)=0$. This equation was solved numerically for τ_2, from which the remaining variables were determined (x, y, τ_3, τ_4, τ_{out}, ϵ_s, ϵ_w, ϵ_b).

The maximization of η_{II} was executed using a Fortran code based on combined secant, Newton–Raphson and bisection methods coupled with a search approach for appropriate initial guesses [5]. The tolerance $|F(\tau_2)| \leq 10^{-6}$ was imposed in order to achieve convergence in all the solutions. The maximization was performed for variable M and fixed parameters (N, τ_H, τ_b, τ_1, U_b/U_s, U_w/U_s). The M range for water on the cold side was $0.01 \leq M \leq 0.5$. The range for toluene (Section 6) was $0.01 \leq M \leq 1$. The chosen discretization was the coarsest set for which the optimal M value did not change as the sets became finer, while the relative error was maintained below 1% in all the cases.

6. Results for toluene as the cold stream

In this section we document the effect of changing the working fluid, by considering the use of toluene instead of water. Now the heat transfer is from the same hot stream as before (exhaust gases, modeled as an ideal gas) to the toluene stream (working fluid).

Toluene is an organic Rankine cycle (ORC) working fluid proposed for the space station power conversion unit [6]. Although organic fluids undergo chemical changes (pyrolytic degradation) when heated to sufficiently high temperatures, in the space station study [6] the predicted degradation of the working fluid inventory was 1% over the 30-year life of the mission. The choice of toluene as working fluid was based on a detailed comparison with regard to cycle efficiency, thermal degradation, chemical and fluid flow properties, flammability, toxicity, experience and availability. Organic fluids reach actual Rankine cycle operating conditions because they undergo phase change at high temperatures, and at pressures much lower than in the case of water.

Since in the unit built and described in Ref. [6] the heating of toluene was at supercritical operating conditions, in this phase of our study we investigated two cases: subcritical and supercritical conditions. In both cases we fixed the cold inlet temperature at $T_1 = 507$ K ($\tau_1 = 1.7$). The inlet temperature of the hot gas was $T_H = 745$ K ($\tau_H = 2.5$). The assumed subcritical pressure was $P_H = 34$ bar (500 psia), which corresponds to the boiling temperature $T_b = 578$ K. The assumed supercritical pressure was $P_H = 40.8$ bar (600 psia). The critical point of toluene is $P_c = 40.6$ bar (592.8 psia) and $T_c = 592$ K. The supercritical unit built in Ref. [6] had $P_H = 41.8$ bar (614 psia) measured at the working fluid outlet. In the numerical work described next, the toluene properties were obtained from available tabulated data as follows: superheated vapor [6], saturation region [7], specific heat of liquid [8,9] and specific heat of vapor [10].

Fig. 12 shows that thermodynamic optima exist in the two toluene cases that we considered. The maximized second law efficiency of the supercritical case is considerably higher than in the subcritical case. Both maxima are distinct, stressing the importance of pinpointing the optimal flow rate of toluene. This result is particularly important in space propulsion, where the minimization of thermodynamic losses subject to weight and volume constraints is crucial. No matter how complicated the actual power plant design might be, the fundamental optimum revealed by Fig. 12 is present, and is worth pursuing.

The effect of the total size of the contact area is documented for the subcritical case in Fig. 13. This figure is similar to Fig. 6 drawn for water. The efficiency increases monotonically as N increases, however the increase in $\eta_{II,max}$ is slow when N is greater than five. The optimal flow rate ratio exhibits a shallow maximum at $\eta_{II,max}$. The area fraction swept by liquid toluene (A_w, or $1-x_{opt}-y_{opt}$) has a shallow maximum at $\eta_{II,max}$. The area fraction for boiling (A_b, y_{opt}) decreases as N increases, while the area fraction for superheating (A_s, x_{opt}) decreases.

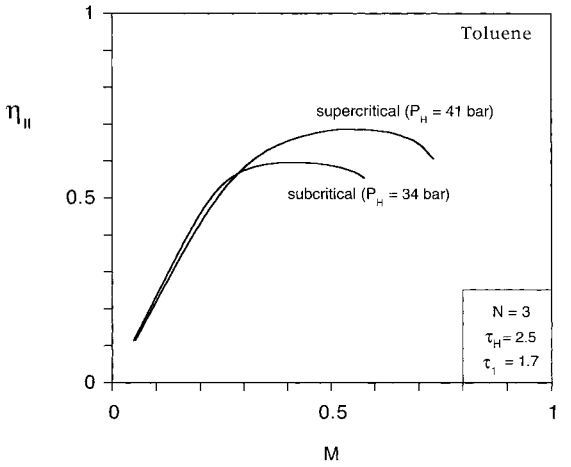

Fig. 12. The maximization of the second law efficiency when the heated stream carries toluene.

7. Concluding remarks

The main conclusion of this study is that the extraction of power from a hot stream can be maximized by

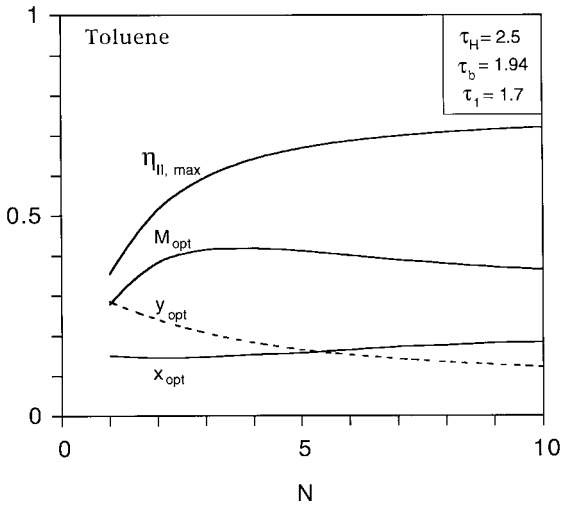

Fig. 13. The effect of the size of the heat transfer area on the thermodynamic optimum with toluene on the cold side of the heat exchanger.

properly matching the stream with a receiving stream of cold fluid, across a finite-size heat transfer area. Proper matching means using a counterflow arrangement where the capacity rate of the cold stream must have a certain value relative to that of the given hot stream (e.g., Fig. 4). This thermodynamic optimum can be located based on the minimization of the total rate of entropy generation subject to the finite-area constraint.

When the cold stream evaporates as it captures a part of the hot-stream exergy, its side of the heat exchanger is divided optimally into three sections: liquid preheating, boiling, and vapor superheating (e.g., Fig. 3). These sections adjust themselves to their proper relative sizes as the system approaches the global thermodynamic optimum.

Important from a practical standpoint is that this optimization principle of matching the streams is general. We showed that the optimal match (M_{opt}) can be located when using either water or toluene on the cold side. We also showed that several of the operating parameters of each design have only a minor impact on the thermodynamic optimum, for example, the size of the heat transfer area (Fig. 6), the inlet temperature of the cold stream (Fig. 7), and the boiling temperature (Fig. 9). These weak effects lend robustness to the optimal design.

This optimization principle can be used widely in the conceptual design of power and refrigeration systems. In Figs. 1 and 2 we chose the simplest setting in which this principle can be demonstrated and pursued. We analyzed the optimal match between two streams, where the colder one undergoes a phase change. This is the case in most power plant design, e.g., Rankine cycle designs. The fundamental problem addressed in this paper is also relevant to more complex designs, such as cogeneration systems, binary cycles, trigeneration systems, and heat recovery boilers.

We focused on the counterflow arrangement (Fig. 2) because this arrangement is optimal thermodynamically [2,11]. Other arrangements, such as parallel flow and cross-flow can be analyzed based on the same method, and in each case an optimal match is to be discovered between the two streams. The limit in which phase change does not occur on the cold side is covered by the fundamental solution reported by Bejan and Errera [11].

In the present method the pressure drops were neglected for the sake of simplicity. Furthermore, the heat exchanger effectiveness (its maximization) was not the objective, which is why the effectiveness was not included in the figures with the numerical results. The maximization of the extraction of exergy from the hot stream was the objective.

We reported results for $M < 1$ because we discovered that in our cases the optima are located in this range. Other applications may require searches over wider ranges of capacity flow rate ratios.

Acknowledgements

The authors acknowledge with gratitude the guidance provided in this research project by Messrs David L. Siems and Gary Runge of the Boeing Corporation. This material is based upon work supported by the Air Force Office of Scientific Research under Contract No. F49620-98-C-0007. Any opinions, findings and conclusions or recommendations are those of the authors and do not necessarily reflect the views of the Air Force Office of Scientific Research. J. C. Ordóñez acknowledges with gratitude the support of the Energy and Thermodynamics Group at Pontificia Bolivariana University (Colombia).

References

[1] A. Bejan, Heat Transfer, Wiley, New York, 1993, Ch. 9.
[2] A. Bejan, Advanced Engineering Thermodynamics, 2nd ed., Wiley, New York, 1997.
[3] J.H. Keenan, F.G. Keyes, P.G. Hill, J.G. Moore, Steam Tables, Wiley, New York, 1969.
[4] A. Bejan, Heat Transfer, Wiley, New York, 1993, p. 24.
[5] D. Kincaid, W. Cheney, Numerical Analysis, Wadsworth, Belmont, CA, 1991.
[6] V. Havens, D. Ragaller, Study of toluene stability for an organic Rankine cycle space-based power system, NASA CR-180884 (microform), 1988.
[7] D. Ambrose, B.E. Broderick, R. Townsend, The vapor pressures above the normal boiling point and the critical pressures of some aromatic hydrocarbons, J. Chem. Soc. London Sec A (1967) 633–641.
[8] D.W. Scott, G.B. Guthrie, J.F. Messerly, S.S. Todd, W.T. Berg, I.A. Hossenlopp, J.P. McCullough, Toluene: thermodynamic properties, molecular vibrations, and internal rotation, J. Phys. Chem. 66 (1962) 911–914.
[9] J.L. San José, G. Mellinger, R.C. Reid, Measurement of the isobaric heat capacity of liquids and certain mixtures above the normal boiling point, J. Chem. Eng. Data 21 (1976) 414–417.
[10] R.C. Reid, J.M. Prausnitz, T.K. Sherwood, The Properties of Gases and Liquids, 3rd ed., McGraw-Hill, New York, 1977.
[11] A. Bejan, M.R. Errera, Maximum power from a hot stream, Int. J. Heat Mass Transfer 41 (1998) 2025–2036.